THE JOURNAL OF PHYSICAL CHEMISTRY C

Article

pubs.acs.org/JPCC

Size Dependence of Temperature-Related Optical Properties of PbS and PbS/CdS Core/Shell Quantum Dots

Haiguang Zhao,[†] Hongyan Liang,[†] François Vidal,[†] Federico Rosei,[†,‡] Alberto Vomiero,[†,‡] and Dongling Ma*[,†]

[†]Institut National de la Recherche Scientifique, INRS-Energie, Matériaux et Télécommunications, 1650 Boulevard Lionel-Boulet, Varennes, Québec J3X 1S2, Canada

[‡]Center for Self-Assembled Chemical Structures, McGill University, Montréal, Québec H3A 2K6, Canada

Supporting Information

ABSTRACT: The effect of PbS core size on the temperature-dependent photoluminescence (PL) of PbS/CdS quantum dots (QDs) in the temperature range of 100−300 K was thoroughly investigated and compared with shell-free PbS QDs. The core/shell QDs show significantly smaller PL intensity variation with temperature at a smaller PbS size, while a larger activation energy when the PbS domain size is relatively large, suggesting both different density and different distribution of defects/traps in the PbS and PbS/CdS QDs. The most remarkable difference consists in the PbS size dependence of the energy gap temperature coefficient (dE/dT). The PbS/CdS QDs show unusual non-monotonic dE/dT variation, resulting in the reversal of the dE/dT difference between the PbS and PbS/CdS QDs at a larger PbS size. In combination with theoretical calculations, we find that, although lattice dilation and carrier-phonon coupling are generally considered as dominant terms, the unique negative contribution to dE/dT from the core/shell interfacial strain becomes most important in the relatively larger-core PbS@CdS QDs.

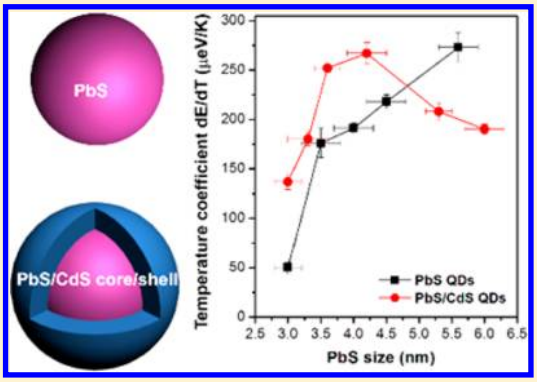

1. INTRODUCTION

Among various kinds of quantum dots (QDs) presenting interesting optical properties in the near-infrared (NIR) spectral region, lead chalcogenide QDs exhibit multiple unique features, such as large exciton Bohr radii (18 nm for PbS, 46 nm for PbSe, and 150 nm for PbTe) and small bulk band gaps (0.41, 0.28, and 0.31 eV at 300 K for PbS, PbSe, and PbTe, respectively), leading to quantum confinement in relatively large-sized QDs with the emission wavelength tuned over a broad NIR range.[1,2] Such QDs may find potential applications in NIR photodetectors, biosensors, deep tissue imaging, and solar cells.[3−6]

For practical applications, QDs are required to exhibit a high quantum yield (QY) and to have good photo- and thermal-stability. However, lead chalcogenide QDs are found to be unstable with respect to the structure at high temperature (in general higher than 100 °C) or even under normal processing or operation conditions. Their optical properties are also quite sensitive to sample status, such as QD dispersion in a medium. Surface oxidation, formation of surface defects/traps, and possible exciton energy transfer to adjacent QDs in closely packed QD systems can lead to the spectral shift of the photoluminescence (PL) band and the reduction of QY of QDs, thus limiting their use in devices.[7−10] The core/shell structure can be designed to stabilize and maximize the fluorescence of the QD core. The shell can serve as a barrier to protect the core against oxidation and removes defects/traps on the core surface by offering better surface passivation. In addition, by using a wider band gap material for the shell, charge carriers can be confined in the core, thus being kept away from the surface and surrounding environment.[8−11] As a result, surface interactions and environmental factors are expected to have limited impact on the fluorescence efficiency and stability of the QD core in the core/shell system.

The synthesis of NIR-emitting core/shell PbSe/CdSe, PbS/CdS, and PbSe/PbS QDs has recently been demonstrated.[8,10,12] The core/shell structure largely enhances the PL and the thermal- and photo- stability of QDs, similarly to the well-known CdSe/ZnS core/shell system.[8,10,12,13] Recent work by Abel and co-workers showed that the thermal activation energy for nonradiative decay of excitons in PbSe/CdSe core/shell QDs could be enhanced by a factor of 4 with respect to bare PbSe QDs.[14] While the similar system of PbS/CdS core/shell QDs was also recently reported,[15] the dependence of its optical behavior on temperature, however, has not been systematically investigated. Moreover, although the CdS shell has been demonstrated to improve the optical properties of the PbS core in PbS/CdS QDs and the effect of CdS shell thickness on basic, constant room-temperature optical properties is known,[15] the effect of core size on the temperature-dependent

Received: April 13, 2014
Revised: August 11, 2014
Published: August 11, 2014

   dx.doi.org/10.1021/jp503617h | J. Phys. Chem. C 2014, 118, 20585−20593

optical properties of QDs remains largely unexplored. In particular, it is unclear how the delocalization of carriers in the core/shell system, partially related to core size, affects the temperature-dependent optical properties of PbS/CdS core/shell QDs.

Here we thoroughly investigate the PL behavior of PbS/CdS QDs of various core sizes with similar shell thicknesses, dispersed in a polymer matrix in the temperature range of 100−300 K. The temperature dependence of PL was investigated by exploring the PL peak energy shift and PL intensity variation and by evaluating the activation energy and energy gap temperature coefficient. These values are compared with those obtained from shell-free PbS QDs. We find that the variation of the optical properties of QDs in the temperature range of 100−300 K is strongly dependent on the size of the core or the size of PbS QDs. Unlike the PbS QDs, the core/shell QDs show unusual size dependence in their energy gap temperature coefficient. We interpret this by taking into account multiple factors, such as quantum confinement and interfacial strain.

2. EXPERIMENTAL SECTION

2.1. Materials. Lead acetate trihydrate, bis(trimethylsilyl) sulfide $(TMS)_2S$ (synthesis grade), trioctylphosphine (TOP, technical grade, 90%), lead chloride (98%), sulfur (100%), oleylamine (OLA) (technical grade, 70%), lead acetate trihydrate, cadmium oxide (99%), oleic acid (OA), poly(methyl methacrylate) (PMMA), and octadecene (ODE) were obtained from Sigma-Aldrich Inc. Hexane, toluene, dimethyl sulfoxide, and ethanol were purchased from Fisher Scientific Company. All chemicals were used as purchased.

2.2. Synthesis. *2.2.1. Synthesis of PbS QDs.* PbS QDs with diameter larger than 3 nm were synthesized by using OLA as ligands.[16,17] Typically, $PbCl_2$ (3.6 mmol) in OLA (2.4 mL) and sulfur (0.36 mmol) in OLA (0.24 mL) were purged, respectively, by N_2 at room temperature for 30 min. The $PbCl_2$−OLA suspension was heated to 160 °C and kept at this temperature for 1 h. The $PbCl_2$−OLA suspension was cooled to 120 °C under vacuum for 15 min. The flask was then reopened, and the N_2 flux was restored. Sulfur in OLA at room temperature was quickly injected into the $PbCl_2$−OLA suspension under vigorous stirring. The reaction cell was quenched with cold water after the growth reaction was conducted at 100 °C for 1−360 min to obtain PbS QDs of different sizes. Ethanol was added, and then the suspension was centrifuged and the supernatant was removed. The QDs were dispersed in toluene. The size of PbS QDs can be tuned from 3.5 to 8 nm by adjusting the molar ratio of Pb/S, injection temperature, and reaction time.

PbS QDs with a diameter of 3.0 nm were synthesized by using OA as ligands.[18] In a typical synthesis, a mixture of lead acetate trihydrate (1 mmol), OA (1.2 mL), and ODE (15 mL) were heated to 150 °C for 1 h. Then, the system was cooled to ∼100 °C under vacuum for 15 min. Subsequently, the solution containing 0.5 mmol $(TMS)_2S$ and 5 mL of ODE was quickly injected into the reaction flask at 130 °C. Finally, the reaction was quenched by cold water. PbS QDs were precipitated by centrifugation following the addition of ethanol to remove unreacted lead oleate and free OA molecules and then redispersed in toluene or chloroform.

2.2.2. Synthesis of PbS@CdS QDs. PbS/CdS QDs were synthesized via a cation-exchange method.[8−10] Typically, CdO (2.3 mmol), OA (2 mL), and ODE (10 mL) were heated to 255 °C under N_2 for 20 min. The clear solution was cooled to 155 °C under vacuum for 15 min. The flask was then reopened, and the N_2 flux was restored. PbS QDs suspension in toluene (1 mL, absorbance = 3 at the first absorption exciton peak) was diluted in 10 mL toluene, bubbled for 30 min, and then heated to 100 °C immediately. The Cd/OA mixture was injected. The reaction cell was quenched with cold water after the growth reaction was conducted at 100 °C for different time. PbS/CdS QDs were precipitated with ethanol and then redispersed in chloroform. The typical shell thickness is around ∼0.6−0.8 nm.

2.3. Ligand Exchange. Ligand exchange was done following the procedures reported in ref 19. The PbS QDs capped with OLA were precipitated and redispersed in OA/toluene. After precipitation with alcohol and centrifugation, the QDs were redispersed in toluene and the ligand exchange was repeated at least twice. Finally, the QDs were redispersed in chloroform.

2.4. QD Concentration. The concentration of purified PbS and PbS/CdS QDs in toluene was determined using Beer−Lambert's law: $A = \varepsilon CL$, where A is the absorbance at the peak position of the first exciton absorption peak for a given sample, C is the molar concentration of QDs, ε is the extinction coefficient per mole of QDs, and L is the light path length.[16] ε was determined using $\varepsilon = 19600\ r^{2.32}$, where r is the radius of QDs, which can be achieved from transmission electron microscopy (TEM) measurements.

2.5. QD Film Preparation. The QDs solution was mixed with PMMA in chloroform and then spin-coated on the glass substrate. The concentration of QDs in this mixture solution was around 1 μM, and the concentration of polymer was 1 wt %.

2.6. Theoretical Calculation of Wave Functions and dE/dT. To calculate the electron and hole wave functions, we solved the stationary Schrödinger equation in spherical geometry, in which we used the bulk values for the effective masses of electrons (m_e*) and holes (m_h*), namely $m_e^* = 0.085m_e$ and $m_h^* = 0.085m_e$ for PbS, and $m_e^* = 0.2m_e$ and $m_h^* = 0.7m_e$ for CdS, where m_e is the electron mass at rest in vacuum.[20] The potentials for electrons and holes as a function of position were approximated as the lowest unoccupied molecular orbital (LUMO) and highest occupied molecular orbital (HOMO) levels, respectively, for the bulk materials.[21] For PbS, these levels are −4.5 and −4.91 eV, respectively, while for CdS they are −3.3 and −5.8 eV, respectively.[20] Outside the QD, the potentials were set as 0 and −9.8 eV for electrons and holes, respectively. The interaction between electrons and holes was neglected in the calculations. By assuming the potentials in the Schrödinger equation are shifted by the amount: $\Delta E = \pm 30 \times T \times D$ (in μeV) where T is the temperature in K and D is the total diameter of the QD in nm, we calculated the dE/dT as a function of PbS core size through the electron−phonon coupling effect. The "+" sign corresponds to the electrons and the "−" sign corresponds to holes. The latter expression is taken from a fit to the dE_g/dT data given in ref 22.

2.7. Characterizations. PbS and PbS/CdS QDs were characterized by a JEOL 2100F TEM. The Pb/Cd ratio was measured by using inductively coupled plasma optical emission spectrometry (ICP-OES) (PerkinElmer Model Optima 7300 DV). The size distribution of QDs was estimated by measuring the size of ∼100−200 QDs for each sample and further modeling it with the Gaussian distribution.

Absorption spectra were acquired with a Cary 5000 UV−vis−NIR spectrophotometer (Varian) with a scan speed of 600

dx.doi.org/10.1021/jp503617h | J. Phys. Chem. C 2014, 118, 20585−20593

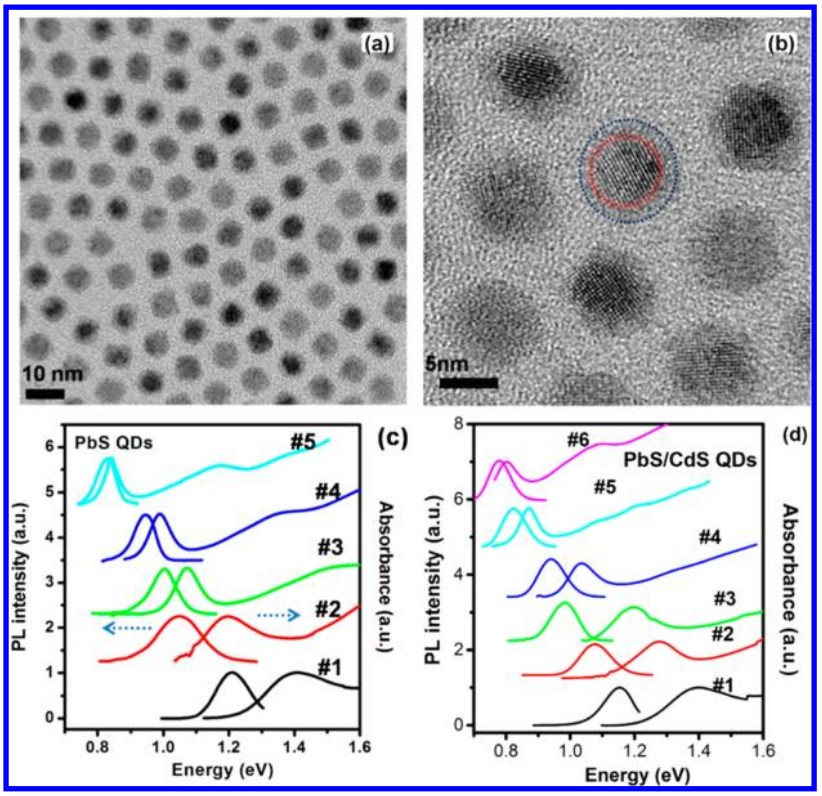

Figure 1. High magnification (a) TEM and (b) HRTEM images of PbS/CdS QDs with an overall average diameter of 6.5 nm. The inset circles of (b) indicate the core and shell regions of PbS/CdS QDs. Representative absorption and emission spectra of (c) PbS and (d) PbS/CdS QDs.

nm/min. Fluorescence spectra were taken with a Fluorolog-3 system (Horiba Jobin Yvon) equipped with a temperature controllor. The excitation wavelength was set at 674 nm.

The temperature-dependent optical properties of PbS and PbS/CdS QDs were measured in the PMMA matrix in the temperature range of 100−300 K by monitoring the variation of their PL spectra with temperature.

3. RESULTS AND DISCUSSION

3.1. Synthesis and Structure of QDs. Colloidal PbS QDs with various sizes were synthesized according to procedures described elsewhere[16−18] and were subsequently used to synthesize PbS/CdS QDs via a cation-exchange approach.[10] The as-synthesized PbS QDs were capped by OLA or OA, depending on the synthesis approach.[16−18] Subsequently, the OLA ligands in OLA-QDs were replaced by OA ligands, which can easily be done due to the stronger binding of OA ligands with the QD surface.[19] The OA-capped PbS QDs were then used as a starting material to synthesize PbS/CdS QDs. Following the cation exchange, the core/shell QDs were also capped with OA because in this approach, only OA was introduced as ligands.[8,9] In the following, all the characterizations were carried out for OA-capped PbS or core/shell QDs. They all exhibit a uniform size distribution (Figure 1, panels a and b, and Figures S1 and S2 of the Supporting Information). High-resolution TEM (HRTEM) confirms that PbS/CdS QDs synthesized via the cation-exchange approach have a core/shell structure. The darker part in the center clearly shows lattice fringes that match the (200) planes of pure PbS, while the lighter part corresponds to the shell (Figure 1b). As we reported previously, the shell is mainly composed of CdS, rather than alloyed $Pb_xCd_{1-x}S$.[10] The average diameter of the PbS QDs was estimated from TEM images. For the core/shell QDs, the Pb-to-Cd atomic ratio was first determined by ICP-OES. Using this ratio and the overall diameter from TEM images, the diameter of the remaining PbS core and thickness of the shell were estimated by using the approach presented in ref 10. The overall QD diameter (d_{total}), core diameter (d_{core}), and CdS shell thickness (d_{shell}) are listed in Table 1. The diameters of PbS and core/shell PbS/CdS QDs range from 3 to 7.4 nm, all showing relatively high PL intensity, indicating that our synthesis yields QDs with good optical properties. In the following, we denote the "bare" PbS QDs with sizes of 3.0, 3.5, 4.0, 4.5, and 5.6 nm as PbS#1, PbS#2, PbS#3, PbS#4, and PbS#5, respectively, and the core/shell PbS/CdS QDs with core sizes of 3.0, 3.3, 3.6, 4.2, 5.3, and 6.0 nm as PbS/CdS#1, PbS/CdS#2, PbS/CdS#3, PbS/CdS#4, PbS/CdS#5, and PbS/

Table 1. Relevant Parameters of the Investigated PbS and PbS/CdS QDs[a]

samples	d_{total} (nm)	d_{core} (nm)	d_{shell} (nm)	E_{abs} (eV)	E_{PL} (eV)
PbS#1	3.0 ± 0.2	–	–	1.41	1.21
PbS#2	3.5 ± 0.3	–	–	1.19	1.04
PbS#3	4.0 ± 0.3	–	–	1.07	0.98
PbS#4	4.5 ± 0.3	–	–	0.99	0.94
PbS#5	5.6 ± 0.3	–	–	0.84	0.83
PbS/CdS#1	4.5 ± 0.3	3.0 ± 0.2	0.8	1.40	1.15
PbS/CdS#2	4.5 ± 0.3	3.3 ± 0.3	0.6	1.28	1.07
PbS/CdS#3	5.5 ± 0.3	3.6 ± 0.2	0.9	1.18	0.98
PbS/CdS#4	5.5 ± 0.3	4.2 ± 0.3	0.7	1.03	0.95
PbS/CdS#5	6.5 ± 0.3	5.3 ± 0.2	0.6	0.87	0.82
PbS/CdS#6	7.5 ± 0.4	6.0 ± 0.3	0.7	0.80	0.78

[a]Energies corresponding to excitonic absorption maximum (E_{abs}) and PL maximum (E_{PL}) for QDs in toluene.

dx.doi.org/10.1021/jp503617h | J. Phys. Chem. C 2014, 118, 20585−20593

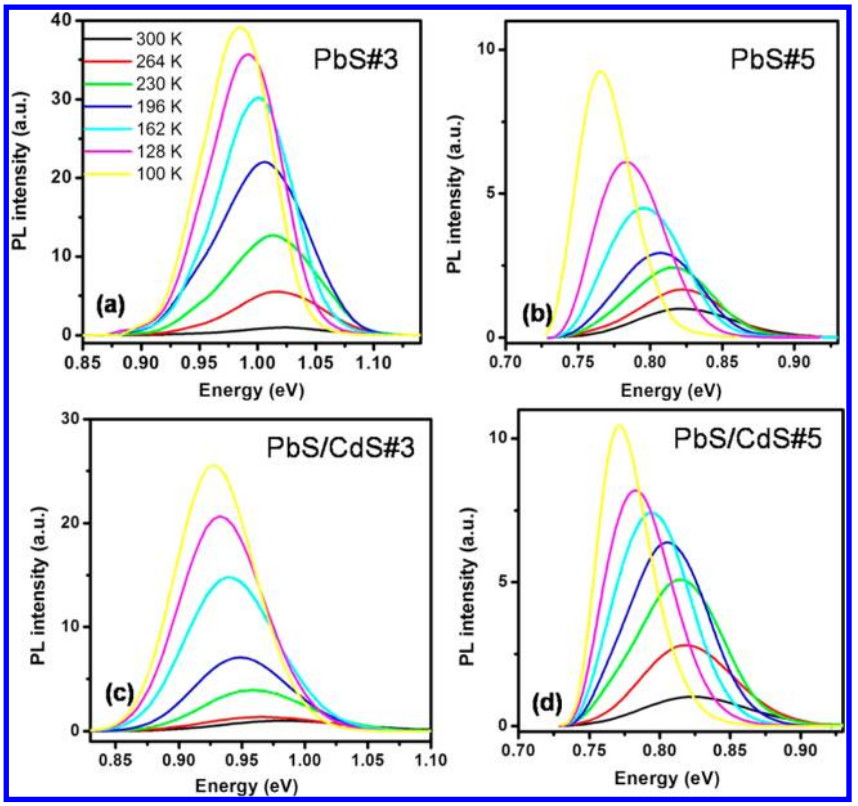

Figure 2. PL spectra of (a) PbS#3, (b) PbS#5, (c) PbS/CdS#3, and (d) PbS/CdS#5 recorded at different temperatures from 300 to 100 K.

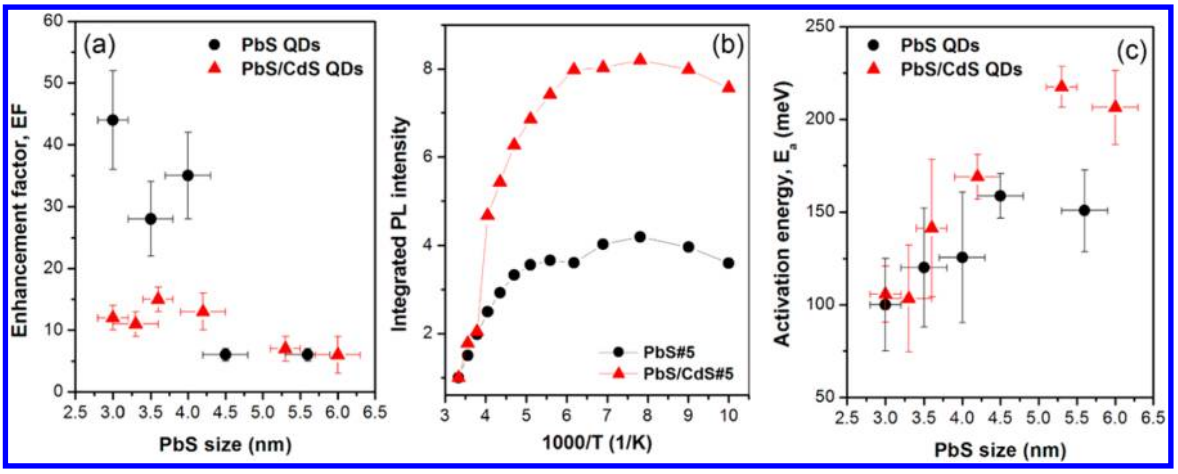

Figure 3. (a) EF of PbS and PbS/CdS QDs as a function of the average diameter of PbS QDs or the average core size of core/shell QDs. (b) Normalized integrated PL intensity of PbS (#5) and PbS/CdS QDs (#5) as a function of 1000/T, where T is temperature. (c) E_a of PbS and PbS/CdS QDs as a function of the average diameter of PbS QDs or the average core size of core/shell QDs. The solid lines in (b) are guides for the eye.

CdS#6, respectively. PbS#4 was used to synthesize PbS/CdS#1 and PbS/CdS#2, and PbS#5 was used to synthesize PbS/CdS#3 and PbS/CdS#4. The PbS QDs with diameter of 6.5 and 7.4 nm were used to synthesize PbS/CdS#5 and PbS/CdS#6, respectively. The representative absorption and PL spectra of several solution samples containing various sizes of PbS and PbS/CdS QDs measured at 300 K are shown in Figure 1 (panels c and d). Both the first excitonic absorption peak and emission peak were clearly observed for these samples. The energies corresponding to the maximum absorption (E_{abs}) of the excitonic absorption band and the PL maximum (E_{PL}) are reported in Table 1.

These colloidal QDs were subsequently mixed with PMMA and spin-coated on glass substrates for PL measurements. To investigate the effect of QD size or core size on the optical properties, for all samples, QD concentration in the PMMA solution (1%) was kept constant at 1 μM. The low concentration of well-dispersed QDs in the polymer matrix in the films minimizes the possible energy transfer events between adjacent QDs, as evidenced by the small emission peak variation (±5 meV) between the measurements performed in solution and in the PMMA film (Figure S3 of the Supporting Information).

3.2. Temperature Effect on PL Quenching. Figure 2 shows the evolution of the PL spectra of representative samples

dx.doi.org/10.1021/jp503617h | J. Phys. Chem. C 2014, 118, 20585−20593

excited at 1.85 eV and recorded at different temperatures from 300 to 100 K. Decreasing temperature systematically leads to the narrowing of the emission peak (Figure S4 of the Supporting Information), the increase of PL intensity, and the red shift of the emission peak energy E for all the samples investigated herein, both in the case of shell-free PbS QDs and core/shell QDs. The decrease of the full width at half-maximum (fwhm) of the PL peak with decreasing temperature is attributed to the suppression of the phonon-carrier interactions.[23−25] Similar narrowing of the PL peak of PbS QDs has also been observed recently by other groups.[23−25] Figure 3b displays the integrated PL intensity of QDs versus inverse temperature ($1000/T$) for PbS#5 and PbS/CdS#5. The plots show a similar trend for all samples, namely, an increase of the PL intensity with decreasing temperature, followed by a plateau in the low temperature range. In general, such temperature-dependent increase of the integrated PL intensity in various types of QDs has been mainly attributed to the suppression of carrier trapping by defects/traps and the phonon-assisted thermal escape.[23,24] Aiming to understand the core size effect on PL enhancement during the temperature decrease, we calculated the PL enhancement factor (EF), according to the following equation:

$$\mathrm{EF} = \frac{I^{\mathrm{PL}}_{100\mathrm{K}}}{I^{\mathrm{PL}}_{300\mathrm{K}}}$$

where $I^{\mathrm{PL}}_{100\mathrm{K}}$ and $I^{\mathrm{PL}}_{300\mathrm{K}}$ are the integrated PL intensity at 100 and 300 K, respectively.

As shown in Figure 3a, the average EF of the PbS QDs is in the range of 30−45 when their size is below 4.5 nm, while it drops down rapidly to ∼6 above 4.5 nm. In contrast, the EF of the core/shell QDs is in the small range of 6−15 and does not show a strong size dependence. The EF values of these QDs are in line with previous reports for shell-free PbS QDs, which showed that EF is typically in the range from one to several tens.[24−26] Higher EF values indicate stronger thermal quenching of the PL emission at higher temperature. Recent studies revealed several major factors that can affect the thermal quenching of the PL emission: (i) the activation/redistribution of carrier recombination centers with temperature; (ii) phonon-assisted thermal escape; and (iii) temperature-dependent energy transfer.[25−29] For example, Gao and Johnson noticed that the emission of PbS QDs during temperature variation was strongly sensitive to carrier recombination centers, which were introduced by the rearrangement of capping ligands on the QD surface during chemical treatments, such as ligand exchange.[26] In another case, Nelson et al. found the mobility of surface capping ligands could be largely affected by temperature, leading to the appearance of liquidlike surface Pb atoms with reduced chemical bonding to the rest of the PbS lattice, thus creating surface electronic traps.[27] These traps led to the strong quenching of PL of the PbS QDs at relatively higher temperature.[27] As mentioned above, in our system the QDs were buried in the PMMA matrix at very low QD concentration, which ideally minimizes the energy and charge transfer between neighboring QDs. In addition, the PL of the QDs in the PMMA film is very stable with respect to their PL peak position and peak shape at room temperature during their storage of as long as several weeks. It suggests the resistance of the QDs to oxidation in the PMMA matrix, as oxidation will cause the blue shift of PL peaks. This finding presumably excludes the possibility of the introduction of defects due to surface oxidation. We hypothesize that the polymer matrix serves as a barrier to protect the QDs from oxidation. However, the PMMA film preparation process led to the decrease of the PL intensity, indicating the introduction of nonradiative recombination centers during this process. Compared to the inorganic shell-free PbS QDs, there are in general less defects in the core/shell QDs due to the better surface passivation by the inorganic CdS shell, as testified by enhanced QY immediately following shell formation.[8,11] This has also been supported by the femtosecond transient absorption spectroscopy study.[30] Moreover, the PL of core/shell QDs is less sensitive to the surface interaction with external environments due to the barrier effect of the CdS shell.[11] As a consequence, the PL of core/shell QDs, as compared to that of pure QDs, is less affected by the introduction of recombination centers on the surface, which is supported by their much lower PL decrease (25% vs 50%) during the film preparation. In the core/shell QDs, the presence of similar density of "effective" nonradiative recombination centers, most likely at the core/shell interface, explains their somewhat similar EF values (Figure 3a). Closer examination shows that the EF values for relatively large core QDs (core > ∼5 nm) are actually slightly smaller, indicative of slightly lower density of the "effective" nonradiative recombination centers on the surface in the larger QDs when they are buried in the PMMA matrix. Further, in comparison with the inorganic shell-free PbS QDs, experimental data show that the core/shell QDs are less sensitive to thermal quenching when the PbS size is relatively small (<4.5 nm) (Figure 3a). This beneficial feature could be reasonably attributed to the lower number of thermally activated traps, and the lower sensitivity to the surface traps of the core/shell QDs. On the other hand, for the PbS QDs themselves, smaller EF values in larger QDs are also consistent with the lower density of "effective" recombination centers in larger QDs when they are encapsulated by PMMA. The lower level of thermal-assisted escape might also be the reason for the lower EF in larger QDs.[31] The size-dependent thermal activation energy (E_a) for PL thermal quenching in the core/shell samples was analyzed in detail and compared with that for the PbS QDs. The integrated PL signal (I_{PL}), which is proportional to the total energy radiated, could be fitted accurately by using the equation $I_{\mathrm{PL}}{}^{-1} = A + B\exp(-E_a/k_BT)$ (Figure S5 of the Supporting Information), where A is the low-temperature limit of $I_{\mathrm{PL}}{}^{-1}$, B is a rate constant, k_B is Boltzmann's constant, and T is the absolute temperature. As shown in Figure S5 of the Supporting Information, a clear Arrhenius-type behavior of the reverse integrated PL as a function of inverse temperature was found in the system of PbS and PbS/CdS QDs, similar to the observation in the system of PbSe/CdSe QDs reported by Abel et al.[14] E_a values obtained from three different batches of QDs are summarized in Figure 3c for each sample. The shell-free PbS QDs show a slight increase in E_a in the range of 100−150 meV with increasing QD size, and then their E_a saturates for larger QD size. The core/shell QDs, instead, show much stronger size-dependent behavior: with the increase of core size from 3.0 to 5.3 nm, E_a increases significantly from ∼100 meV to ∼220 meV, and then it remains almost constant with further core size increase.

Generally, the thermal activation energy could result from the effects of potential barrier, exciton binding energy, defect/trap states, and exciton−phonon interactions.[23,28,29] In our case, smaller QDs are expected to have higher density of defects/trap states on the surface following the film sample

dx.doi.org/10.1021/jp503617h | J. Phys. Chem. C 2014, 118, 20585−20593

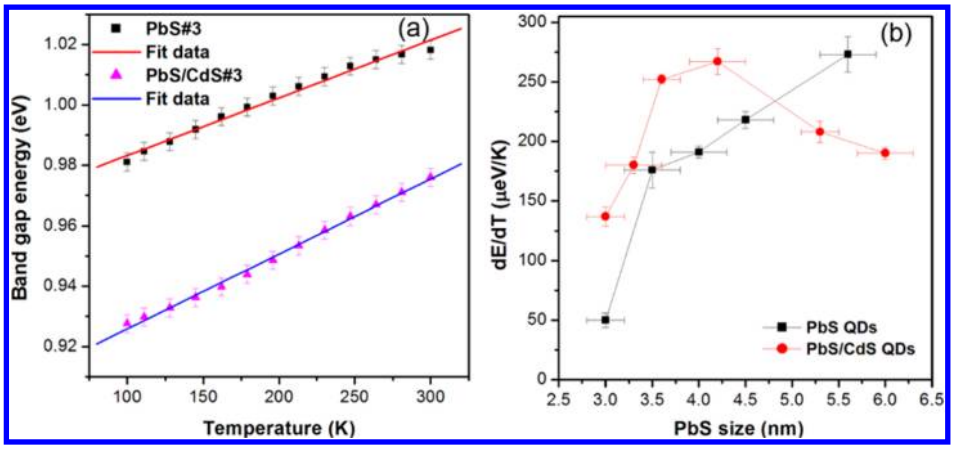

Figure 4. (a) PL peak energy of PbS and PbS/CdS QDs as a function of temperature. (b) Temperature coefficient dE/dT of PbS and PbS/CdS QDs with respect to the diameter of PbS QDs or PbS cores. The solid lines in (b) are guides to the eye.

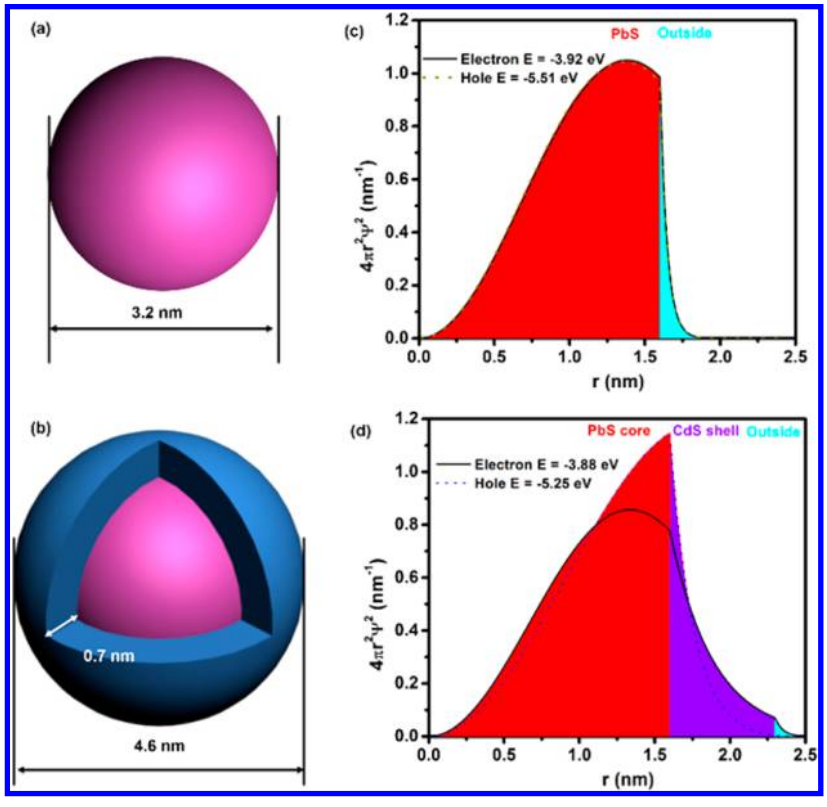

Figure 5. Radial distribution functions for 1S electron and hole of a PbS QD with a size of 3.2 nm in diameter and of a PbS/CdS core/shell QD with a core size of 3.2 nm in diameter and a shell thickness of 0.7 nm.

preparation. As mentioned above, these defect/trap states serve as nonradiative carrier recombination centers, offering PL quenching channels and therefore reducing E_a. An interesting observation is, for larger PbS size, the PbS and PbS/CdS QDs show the similar EF while the latter exhibit considerably higher E_a. It discloses the different distributions of the defect/trap states in these two systems. The significant higher E_a of the core/shell QDs, when the PbS size is relatively large, indicates much higher thermal stability of the PL of the core−shell system.

3.3. Temperature Effect on the Energy Gap of QDs. In the following, we discuss the temperature effect on the energy gap E of QDs. For both PbS and PbS/CdS core/shell QDs this energy E, estimated from the energy of the emission peak, exhibits a linear dependence on temperature (Figure 4a), a behavior that has already been observed for PbS QDs in the same temperature range by others (100−300 K).[32] The temperature coefficients dE/dT, obtained from the emission peak energy versus T plots, are shown in Figure 4b. It can be seen that the dE/dT of PbS QDs monotonically increases with increasing size and finally approaches the value of 260 μeV/K, similar to previously reported values for PbS QDs.[22] Unusual behavior was observed for the core/shell PbS/CdS QDs. The initial increasing trend of the dE/dT reverses when the PbS core size becomes larger than ∼4.5 nm, which eventually leads to lower dE/dT than that of the shell-free PbS QDs, although the dE/dT of the core/shell QDs is higher than that of the PbS QDs when the PbS size is relatively small.

dx.doi.org/10.1021/jp503617h | J. Phys. Chem. C 2014, 118, 20585−20593

dE/dT of PbS QDs has dominant contributions from lattice dilation and electron−phonon interactions.[22,33] Additional contributions might arise from mechanical strain and thermal expansion of the wave function envelope.[22] As all the PbS QDs and PbS/CdS QDs are buried in the polymer matrix, the contribution from mechanical strain between the polymer and QDs due to different levels of thermal expansion is supposed to affect PbS and PbS/CdS QDs similarly. Therefore, the different behavior observed for PbS and PbS/CdS QDs may originate from the formation of the core/shell structure, which introduces different electron−phonon coupling and lattice dilation from those in the PbS QDs, and moreover, the unique strain at the interface between the PbS core and the CdS shell in the core/shell QDs.

First, we focus the discussion on the effect of electron−phonon coupling in PbS/CdS core/shell QDs on dE/dT. It is known that the contribution from the electron−phonon coupling to dE/dT is strongly correlated to the quantum confinement effect of QDs, and in general, it is expected to decrease with decreasing size simply due to the increase of the spacing between quantum-confined energy levels,[21,33] consistent with the trend we observed for PbS QDs (Figure 4b). The core/shell QDs, however, show a different trend, and also their dE/dT is higher than that of the PbS QDs when the PbS size is relatively small. To understand the observed difference, we calculated the electron and hole wave functions of a PbS QD (3.2 nm in diameter) and a PbS/CdS QD (core diameter: 3.2 nm; shell thickness: 0.7 nm) (Figure 5). In these calculations, we used the effective mass of electrons and holes in bulk PbS and CdS and the band structure of bulk CdS.[34] Figure 5 (panels c and d) shows the radial distribution functions of 1S electron and hole in these two QDs as a function of the radial distance with respect to the QD center. For PbS/CdS, it seems that both electrons and holes have a high probability to penetrate deeply into the CdS layer and some further outside the QD, although their amplitudes decay throughout the shell thickness. As higher fractions of the electrons and holes in the core/shell QDs can in theory extend out of the PbS domain with respect to those of the shell-free PbS QDs having the same PbS size, the quantum confinement energy is expected to be smaller in the core/shell QDs, which may explain their higher dE/dT values in most cases.

This explanation was further supported by the calculation of the part of dE/dT arising solely from the electron−phonon coupling as a function of PbS size (Figure S6 of the Supporting Information) (the calculation details are shown in the Supporting Information). Although the calculated values are much higher, the predicted trend is in agreement with most of our experimental results [except for the core/shell QDs with relatively large core size (>4.5 nm)] and this trend is also consistent with the results of Olkhovets et al.[22] The calculated dE/dT of PbS/CdS QDs in our investigated size range is consistently higher than that of PbS QDs due to the decrease of quantum confinement in the former. Similar results have been reported for the core/shell structured PbSe/PbS and PbSe/PbS_xSe_{1-x} QDs, in which the electron−phonon coupling was considered to be a dominant factor responsible for the reduction of dE/dT in the core/shell QDs.[12] However, this explanation based on the quantum confinement effect and the calculation results shown in Figure S6 of the Supporting Information are consistent with experimental observations for QDs with the PbS size below 4.5 nm. The unusual phenomenon observed for the larger core/shell QDs calls for other mechanisms to be taken into account.

Olkhovets et al.[22] identified four different contributions to dE/dT in lead-salt QDs: thermal expansion of the lattice, electron−phonon coupling, thermal expansion of the wave function envelope, and mechanical strain. It is suggested that the first two contributions (which generally dominate for shell-free QDs) are positive, while the last two are negative. Our observation of the decrease of dE/dT for large core size in the PbS/CdS system could be explained either by a slower increase of the positive contributions to dE/dT for larger QD size or by a faster increase of the negative contributions. The (negative) contribution of the thermal expansion of the wave function envelope is estimated to decrease as the QD size increases[22] and is thus likely not the factor explaining our observations. In comparison to the inorganic shell-free PbS QDs surrounded by PMMA, the PbS cores in the core/shell QDs are surrounded by the harder material of CdS. With further considering that the thermal-expansion coefficient of PbS is ∼5-fold larger than that of CdS (PbS: 20×10^{-6} K^{-1} vs CdS: 4.1×10^{-6} K^{-1} Å),[35,36] the lattice dilation of the PbS cores with temperature must be limited by the presence of the CdS shell. As a result, the contribution from the lattice dilation to dE/dT is likely to be smaller in the core/shell system as compared to that in the PbS QDs. In addition, the contribution from the lattice dilation is anticipated to be size-dependent, since larger PbS-core QDs suffer more thermal expansion limitation, when the shell thickness is the same, as in the current case, leading to the lower contribution from the lattice dilation to dE/dT in larger core QDs. On the other hand, for the core/shell QDs, the interface strain due to the lattice mismatch (PbS: rock salt, a = 5.93 Å at 300 K[9]; CdS: zinc blende, a = 5.82 Å at 300 K[9]) and due to the different thermal expansion between the core and shell may also affect their dE/dT.[37] The interface strain due to the lattice mismatch at the core and shell interface is likely similar regardless of PbS core size. However, in the radial direction, the mechanical strain due to thermal pressure is expected to be larger for larger core QDs, which could then contribute more negatively to dE/dT (although the size-dependence was estimated to be small in ref 22). The abnormal, non-monotonic temperature-dependence of dE/dT in the core/shell QDs and the resulting final reversal of the difference of dE/dT between the inorganic shell-free QDs and core/shell QDs could well be the consequence of the interplay between all of these factors. As the contributions from these factors are entangled, it is difficult to quantitatively resolve each individual contribution.

■ CONCLUSIONS AND PERSPECTIVES

We thoroughly investigated the temperature-dependent optical properties of a series of PbS and PbS/CdS core/shell QDs with different PbS domain size by exploring PL peak energy shift, PL intensity variation, activation energy for PL quenching, and energy gap temperature coefficient in the temperature range of 100−300 K. The enhancement factor EF of the PbS QDs is in the range of 30−45 when the size is below 4.5 nm in diameter, while it drops to ∼6 above 4.5 nm. For the core/shell QDs, the EF values remain similar in the range of 6−15, due to the overall lower density of recombination centers in these QDs and their lower sensitivity to surface status. Both smaller core/shell and PbS QDs exhibit clear size-dependent activation energy E_a for PL thermal quenching, while E_a becomes more or less constant for a larger PbS size. The considerably larger E_a

dx.doi.org/10.1021/jp503617h | J. Phys. Chem. C 2014, 118, 20585−20593

values for the core−shell QDs as compared to those for the PbS QDs in certain cases suggest different distributions of the effect/trap states in these two systems. An interesting phenomenon was observed for the PbS size dependence of the energy gap temperature coefficient dE/dT. While the PbS QDs exhibit the expected monotonic increase in dE/dT with increasing PbS size, the core/shell QDs show unusual behavior. Their dE/dT decreases after an initial increase with the increases of PbS core size, resulting in eventually lower dE/dT than that of the shell-free PbS QDs. The unexpected PbS size-dependence of dE/dT in the core/shell QDs and their smaller dE/dT than that of the PbS QDs at larger PbS size are mainly attributed to the larger, negative contribution from the interfacial strain in the larger-core core/shell QDs. The slower increase of dE/dT associated with lattice dilatation for larger QDs may also contribute to the observed behavior. The absolute value of dE/dT can be the consequence of the interplay between many factors so that it is difficult to identify each individual contribution. Our work provides new fundamental knowledge on core/shell QDs and paves the way for their exploitation in the NIR region with improved optical features and improved stability with respect to present PbS QDs in, for instance, excitonic solar cells, NIR light-emitting diodes, and NIR biosensors.

■ ASSOCIATED CONTENT

Supporting Information

TEM images, Size distribution of PbS and PbS/CdS core/shell QDs, PL spectra of PbS in solution and film, PL fwhm of PbS and PbS/CdS QDs as a function of temperature, normalized reverse integrated PL intensity of PbS and PbS/CdS QDs as a function of temperature, and calculated temperature coefficient dE/dT of PbS and PbS/CdS QDs. This material is available free of charge via the Internet at http://pubs.acs.org.

■ AUTHOR INFORMATION

Corresponding Author

*E-mail: ma@emt.inrs.ca.

Notes

The authors declare no competing financial interest.

■ ACKNOWLEDGMENTS

D.M. and F.R. greatly appreciate the financial support from NSERC, Canadian Solar Inc., and OLA Display Corp. in the context of a NSERC-Strategic grant. F.R. is grateful to the Canada Research Chairs program for partial salary support. F.R. and D.M. acknowledge funding from MDEIE for an international collaboration grant. A.V. is thankful to the European Union for partial salary support under contract N°299490, Marie Curie International Outgoing Fellowship and for partial funding under contract N°295216, IRSES. H.L. acknowledges FRQNT for a graduate fellowship.

■ REFERENCES

(1) Alivisatos, A. P. Semiconductor Clusters, Nanocrystals, and Quantum Dots. *Science* **1996**, *271*, 933−937.

(2) Rogach, A. L.; Eychmüller, A.; Hickey, S. G.; Kershaw, S. V. Infrared-Emitting Colloidal Nanocrystals: Synthesis, Assembly, Spectroscopy, and Applications. *Small* **2007**, *3*, 536−557.

(3) Konstantatos, G.; Howard, I.; Fischer, A.; Hoogland, S.; Clifford, J.; Klem, E.; Levina, L.; Sargent, E. H. Ultrasensitive Solution-Cast Quantum Dot Photodetectors. *Nature* **2006**, *442*, 180−183.

(4) Michalet, X.; Pinaud, F. F.; Bentolila, L. A.; Tsay, J. M.; Doose, S.; Li, J. J.; Sundaresan, G.; Wu, A. M.; Gambhir, S. S.; Weiss, S. Quantum Dots for Live Cells, in Vivo Imaging, and Diagnostics. *Science* **2005**, *307*, 538−544.

(5) Weissleder, R. Progress Continues in the Development of Smaller, More Penetrable Probes for Biological Imaging. *Nat. Biotechnol.* **2001**, *19*, 316−317.

(6) Tang, J.; Kemp, K. W.; Hoogland, S.; Jeong, K. S.; Liu, H.; Levina, L.; Furukawa, M.; Wang, X.; Debnath, R.; Cha, D.; Chou, K. W.; Fischer, A.; Amassian, A.; Asbury, J. B.; Sargent, E. H. Colloidal-Quantum-Dot Photovoltaics Using Atomic-Ligand Passivation. *Nat. Mater.* **2011**, *10*, 765−771.

(7) Pietryga, J. M.; Schaller, R. D.; Werder, D.; Stewart, M. H.; Klimov, V. I.; Hollingsworth, J. A. Pushing the Band Gap Envelope: Mid-Infrared Emitting Colloidal PbSe Quantum Dots. *J. Am. Chem. Soc.* **2004**, *126*, 11752−11753.

(8) Pietryga, J.; Werder, D.; Williams, D.; Casson, J.; Schaller, R.; Klimov, V.; Hollingworth, J. Utilizing the Lability of Lead Selenide to Produce Heterostructured Nanocrystals with Bright, Stable Infrared Emission. *J. Am. Chem. Soc.* **2008**, *130*, 4879−4885.

(9) Kovalenko, M. V.; Schaller, R. D.; Jarzab, D.; Loi, M. A.; Talapin, D. V. Inorganically Functionalized PbS−CdS Colloidal Nanocrystals: Integration into Amorphous Chalcogenide Glass and Luminescent Properties. *J. Am. Chem. Soc.* **2007**, *129*, 11354−11355.

(10) Zhao, H. G.; Wu, N.; Chaker, M.; Ma, D. Towards Controlled Synthesis and Better Understanding of Highly Luminescent PbS/CdS Core/Shell Quantum Dots. *J. Mater. Chem.* **2011**, *21*, 8898−8904.

(11) Zhao, H. G.; Wang, D. F.; Zhang, T.; Chaker, M.; Ma, D. Two-step Synthesis of High-Quality Water-soluble Near-Infrared Emitting Quantum Dots via Amphiphilic Polymers. *Chem. Commun.* **2010**, *46*, 5301−5303.

(12) Maikov, G. I.; Vaxenburg, R.; Sashchiuk, A.; Lifshitz, E. Composition-Tunable Optical Properties of Colloidal IV−VI Quantum Dots, Composed of Core/Shell Heterostructures with Alloy Components. *ACS Nano* **2010**, *4*, 6547−6556.

(13) Dabbousi, B. O.; Rodriguez-Viejo, J.; Mikulec, F. V.; Heine, J. R.; Mattoussi, H.; Ober, R.; Jensen, K. F.; Bawendi, M. G. (CdSe)ZnS Core-shell Quantum Dots: Synthesis and Optical and Structural Characterization of a Size Series of Highly Luminescent Materials. *J. Phys. Chem. B* **1997**, *101*, 9463−9475.

(14) Abel, K. A.; Qiao, H.; Young, J. F.; van Veggel, F. C. J. M. Four-Fold Enhancement of the Activation Energy for Nonradiative Decay of Excitons in PbSe/CdSe Core/Shell versus PbSe Colloidal Quantum Dots. *J. Phys. Chem. Lett.* **2010**, *1*, 2334−2338.

(15) Zhao, H. G.; Chaker, M.; Ma, D. Effect of CdS Shell Thickness on the Optical Properties of Water-Soluble Amphiphilic Polymer Encapsulated PbS/CdS Quantum Dots. *J. Mater. Chem.* **2011**, *21*, 17483−17491.

(16) Cademartiri, L.; Montanari, E.; Calestani, G.; Migliori, A.; Guagliardi, A.; Ozin, G. A. Size-Dependent Extinction Coefficients of PbS Quantum Dots. *J. Am. Chem. Soc.* **2006**, *128* (31), 10337−10346.

(17) Zhao, H. G.; Chaker, M.; Ma, D. Bimodal Photoluminescence during the Growth of PbS Quantum Dots. *J. Phys. Chem. C* **2009**, *113*, 6497−6504.

(18) Zhang, T.; Zhao, H. G.; Riabinina, D.; Chaker, M.; Ma, D. Concentration-Dependent Photoinduced Photoluminescence Enhancement in Colloidal PbS Quantum Dot Solution. *J. Phys. Chem. C* **2010**, *114* (22), 10153−10159.

(19) Moreels, I.; Justo, Y.; De Geyter, B.; Haustraete, K.; Martins, J. C.; Hens, Z. Size-Tunable, Bright, and Stable PbS Quantum Dots: A Surface Chemistry Study. *ACS Nano* **2011**, *5*, 2004−2012.

(20) Gopidas, K. R.; Bohorquez, M.; Kamat, P. V. Photophysical and Photochemical Aspects of Coupled Semiconductors: Charge-Transfer Processes in Colloidal Cadmium Sulfide-Titania and Cadmium Sulfide-silver(I) Iodide Systems. *J. Phys. Chem.* **1990**, *94* (16), 6435−6440.

(21) De Geyter, B.; Justo, Y.; Moreels, I.; Lambert, K.; Smet, P. F.; Van Thourhout, D.; Houtepen, A. J.; Grodzinska, D.; Donega, C. D. .; Meijerink, A.; Vanmaekelbergh, D.; Hens, Z. The Different Nature of

Band Edge Absorption and Emission in Colloidal PbSe/CdSe Core/Shell Quantum Dots. *ACS Nano* **2010**, *5*, 58−66.
(22) Olkhovets, A.; Hsu, R. C.; Lipovskii, A.; Wise, F. W. Size-Dependent Temperature Variation of the Energy Gap in Lead-Salt Quantum Dots. *Phys. Rev. Lett.* **1998**, *81*, 3539−3542.
(23) Lewis, J. E.; Wu, S.; Jiang, X. J. Unconventional Gap State of Trapped Exciton in Lead Sulfide Quantum Dots. *Nanotechnology* **2010**, *21*, 455402.
(24) Nordin, M. N.; Li, J.; Clowes, S. K.; Curry, R. J. Temperature Dependent Optical Properties of PbS Nanocrystals. *Nanotechnology* **2012**, *23* (27), 275701.
(25) Turyanska, L.; Patane, A.; Henini, M.; Hennequin, B.; Thomas, N. R. Temperature Dependence of the Photoluminescence Emission from Thiol-Capped PbS Quantum Dots. *Appl. Phys. Lett.* **2007**, *90*, 101913.
(26) Gao, J.; Johnson, J. C. Charge Trapping in Bright and Dark States of Coupled PbS Quantum Dot Films. *ACS Nano* **2011**, *6*, 3292−3304.
(27) Nelson, C. A.; Zhu, X. Y. Reversible Surface Electronic Traps in PbS Quantum Dot Solids Induced by an Order−Disorder Phase Transition in Capping Molecules. *J. Am. Chem. Soc.* **2012**, *134* (18), 7592−7595.
(28) Andreakou, P.; Brossard, M.; Li, C.; Bernechea, M.; Konstantatos, G.; Lagoudakis, P. G. Size- and Temperature-Dependent Carrier Dynamics in Oleic Acid Capped PbS Quantum Dots. *J. Phys. Chem. C* **2013**, *117*, 1887−1892.
(29) Chon, B.; Bang, J.; Park, J.; Jeong, C.; Choi, J. H.; Lee, J.; Joo, T.; Kim, S. Unique Temperature Dependence and Blinking Behavior of CdTe/CdSe (Core/Shell) Type-II Quantum Dots. *J. Phys. Chem. C* **2011**, *115*, 436−442.
(30) Wheeler, D. A.; Fitzmorris, B. C.; Zhao, H.; Ma, D.; Zhang, J. Z. Ultrafast Exciton Relaxation Dynamics of PbS and Core/Shell PbS/CdS Quantum Dots. *Sci. China Chem.* **2011**, *54*, 2009−2015.
(31) Jing, P.; Zheng, J.; Ikezawa, M.; Liu, X.; Lv, S.; Kong, X.; Zhao, J.; Masumoto, Y. Temperature-Dependent Photoluminescence of CdSe-Core CdS/CdZnS/ZnS-Multishell Quantum Dots. *J. Phys. Chem. C* **2009**, *113*, 13545−13550.
(32) Valerini, D.; Cretí, A.; Lomascolo, M.; Manna, L.; Cingolani, R.; Anni, M. Temperature Dependence of the Photoluminescence Properties of Colloidal CdSe/ZnS Core/Shell Quantum Dots Embedded in a Polystyrene Matrix. *Phys. Rev. B* **2005**, *71*, 235409.
(33) Wise, F. W. Lead Salt Quantum Dots: The Limit of Strong Quantum Confinement. *Acc. Chem. Res.* **2000**, *33*, 773−780.
(34) Haus, J. W.; Zhou, H. S.; Honma, I.; Komiyama, H. Quantum Confinement in Semiconductor Heterostructure Nanometer-Size Particles. *Phys. Rev. B* **1993**, *47*, 1359−1365.
(35) Browder, J. S.; Ballard, S. S. Thermal Expansion Measurements on Four Optical Materials from Room Temperature to 10 K. *Appl. Opt.* **1972**, *11*, 841−843.
(36) Harbecke, G.; Madelung, O.; Rössler, U. In *Numerical Data and Functional Relationships in Science and Technology*; Landolt-Börnstein, New Series, Group III, Condensed Matter 41C; Springer: Berlin, 1982.
(37) Schwarzl, T.; Kaufmann, E.; Springholz, G.; Koike, K.; Hotei, T.; Yano, M. Temperature-Dependent Midinfrared Photoluminescence of Epitaxial PbTe/CdTe Quantum Dots and Calculation of the Corresponding Transition Energy. *Phys. Rev. B* **2008**, *78*, 165320.